IOPscience iopscience.iop.org

Home Search Collections Journals About Contact us My IOPscience

Symmetry groups for 3D dynamical systems

This article has been downloaded from IOPscience. Please scroll down to see the full text article.

2007 J. Phys. A: Math. Theor. 40 5597

(http://iopscience.iop.org/1751-8121/40/21/011)

View the table of contents for this issue, or go to the journal homepage for more

Download details:
IP Address: 171.66.16.109
The article was downloaded on 03/06/2010 at 05:12

Please note that terms and conditions apply.

J. Phys. A: Math. Theor. **40** (2007) 5597–5620 doi:10.1088/1751-8113/40/21/011

Symmetry groups for 3D dynamical systems

Christophe Letellier[1] **and Robert Gilmore**[2]

[1] Groupe d'Analyse TOpologique et de MOdélisation de SYstèmes Dynamiques, CORIA UMR 6614—Université de Rouen, Av de l'Université, BP 12, F-76801 Saint-Etienne du Rouvray cedex, France
[2] Physics Department, Drexel University, Philadelphia, PA 19104, USA

Received 17 January 2007, in final form 23 March 2007
Published 8 May 2007
Online at stacks.iop.org/JPhysA/40/5597

Abstract
We present a systematic way to construct dynamical systems with a specific symmetry group **G**. Each symmetric strange attractor has a unique image attractor that is locally identical to it but different at the global topological level. Image attractors can be lifted to many inequivalent covering attractors. These are distinguished by an index that has related topological, algebraic and group theoretical interpretations. These methods are used to describe dynamical systems with symmetry groups $\mathbf{V}_4$, $\mathbf{S}_4$ and $\mathbf{S}_6$.

PACS number: 05.45.−a

(Some figures in this article are in colour only in the electronic version)

1. Introduction

In this work, we continue and extend our study of dynamical systems on $\mathbb{R}^3$ with symmetry and closely related dynamical systems without symmetry [1–3]. The two types of systems are related by a local diffeomorphism. This is a differentiable mapping that is 1:1 almost everywhere. The Jacobian of the transformation between the two coordinate systems is singular only on zero- and one-dimensional subsets of the phase space $\mathbb{R}^3$. Such mappings are conveniently constructed with the aid of symmetry groups. In fact, there is a very close relation between symmetry groups, local diffeomorphisms, and strange attractors with and without symmetry [1].

In previous works, we have studied the cover and image relation for groups with two-fold symmetry, such as the rotation group $\mathbf{R}_Z(\pi)$ and the inversion group $\mathbf{P}$, acting in $\mathbb{R}^3$ [1]. We have also studied the cover-image relation for n-fold rotation groups of the type $\mathbf{C}_n$ [3, 4]. In this work, we apply these results to dynamical systems with more complicated symmetry groups, in particular the groups $\mathbf{V}_4$, $\mathbf{S}_4$ and $\mathbf{S}_6$.

In section 2, we summarize the properties of dynamical systems $\dot{X} = F(X)$ with a finite symmetry group. We constrain ourselves especially to three-dimensional dynamical systems, since their global structure is by now rather well understood and they can be explained

 © 2007 IOP Publishing Ltd Printed in the UK

in terms of relatively simple structures called branched manifolds [5–7]. In section 3, we summarize the methods used to construct dynamical systems invariant under a given symmetry group **G**. This is done in particular for the four-group $\mathbf{V}_4$. The tools involve invariant and covariant polynomials [8], invariant coordinates and functions of these coordinates, Jacobians of transformations and the chain rule of elementary calculus. We also introduce more sophisticated concepts, such as the index [1] that distinguishes topologically inequivalent symmetric covers from each other. The index is described in terms of its topological, algebraic and group theoretic properties. We wrap up this section by constructing all the topologically inequivalent covers of the Rössler dynamical system [9] that have $\mathbf{V}_4$ symmetry. There are essentially six inequivalent types of covers.

In sections 4, 5 and 6, we discuss equivariant systems that have been previously introduced. These have symmetry groups $\mathbf{V}_4$ (section 4), $\mathbf{S}_4$ (section 5) and $\mathbf{S}_6$ (section 6). The study of these dynamical systems is considerably simplified by the methods introduced as well as the relation between the strange attractors with symmetry and their images without. Finally, section 7 contains a discussion of our results and some concluding remarks.

2. Review of invariance and equivariance properties

A dynamical system $\dot{X} = F(X), X \in \mathbb{R}^n$ is invariant under a group **G** if it satisfies $\gamma\dot{X} = \gamma F(X) = F(\gamma X), \gamma \in \mathbf{G}$. This can be expressed equivalently as $\gamma F = F\gamma$ or $\gamma F\gamma^{-1} = F$. The functions $F(X)$ are said to be equivariant under the action of the group **G** [10], while the dynamical system $\dot{X} = F(X)$ is invariant under **G**.

For a dynamical system invariant under the action of a finite group **G**, dynamics in the neighbourhood of a point $X \in \mathbb{R}^n$ looks the same as dynamics in the neighbourhood of its image $\gamma X, \gamma \in \mathbf{G}$. This observation has the following specific implications [1].

(1) If X_0 is a fixed point, then γX_0 is a fixed point. At a fixed point, $F(X_0) = 0$. As a result, $F(\gamma X_0) = \gamma F(X_0) = \gamma 0 = 0$.

(2) The Jacobian $[\partial F_i/\partial X_j]_{X_0}$ is related by a similarity transformation to the Jacobian at the image point

$$\left[\frac{\partial F_i}{\partial X_j}\right]_{\gamma X_0} = \gamma \left[\frac{\partial F_i}{\partial X_j}\right]_{X_0} \gamma^{-1}. \tag{1}$$

As a result, if X_0 and γX_0 are fixed points, the eigenvalues of the Jacobians at X_0 and γX_0 are identical. Symmetry-related fixed points have identical stability properties. In addition, the eigenvectors of the two Jacobians are related by the similarity transformation γ.

(3) If X_0 is a fixed point that is left invariant under γ, then the Jacobian evaluated at that fixed point commutes with $\gamma : \left[\frac{\partial F_i}{\partial X_j}\right]_{X_0} = \gamma\left[\frac{\partial F_i}{\partial X_j}\right]_{X_0}\gamma^{-1}$.

(4) If $\phi(t) = (\phi_1(t), \phi_2(t), \ldots, \phi_n(t))$ is a solution to $\mathrm{d}X_i/\mathrm{d}t = F_i(x)$ at X_0, then $\gamma\phi(t) = (\tilde{\phi}_1(t), \tilde{\phi}_2(t), \ldots, \tilde{\phi}_n(t)), \tilde{\phi}_i(t) = \gamma_i^j\phi_j(t)$, is a solution to $\mathrm{d}X_i/\mathrm{d}t = F_i(x)$ at γX_0.

(5) If X_0 is on a closed orbit $\phi(t)$, then γX_0 is on the closed orbit $\tilde{\phi}(t) = \gamma\phi(t)$. If $\phi(t)$ has period T, so that $\phi(t+T) = \phi(t)$, then $\tilde{\phi}(t)$ also has period T. The points X_0 and γX_0 may be on different orbits or on the same orbit. If they are on the same orbit, $\tilde{\phi}(t) = \phi(t+\tau)$, where $k\tau = T$ and k is an integer, $k > 1$ when $\gamma \neq \mathbb{I}$.

(6) If X_0 is 'in' a strange attractor, γX_0 is also. By 'in' we mean that X_0 lies in the closure of a strange attractor (the ω-limit set of the flow). This includes all the unstable periodic orbits associated with (in) the strange attractor.

(7) A strange attractor can consist of one connected component or several disconnected components. In the latter case, if one disconnected component is mapped into itself by group operations $h_i \in \mathbf{H} \subset \mathbf{G}$, this component is mapped into distinct disjoint components by coset representatives $\omega_j \in \mathbf{G}/\mathbf{H}$.

A word on notation. Throughout this work, we discuss the relation between dynamical systems invariant under a group **G** and their image dynamical systems invariant under a group that is a homomorphic image of **G**, in all cases the identity **I**. We distinguish these two cases by use of capital letters in the case of the former, and lower case letters in the case of the latter. We systematically refer to the former as symmetric dynamical systems and the latter as image dynamical systems.

3. Covers with $\mathbf{V}_4$ symmetry

The four-group $\mathbf{V}_4$ (vierergruppe) has four group operations, the identity, two generators, σ_1 and σ_2, and their product $\sigma_1\sigma_2$. The generators satisfy the relations $\mathbb{I} = \sigma_1^2 = \sigma_2^2 = (\sigma_1\sigma_2)^2$. This group can be implemented in $\mathbb{R}^3$ as the group of rotations by π radians about the X-, Y- and Z-axes. The matrix representation of the three rotations in this group is

$$\begin{matrix} R_X(\pi) \\ \begin{bmatrix} +1 & 0 & 0 \\ 0 & -1 & 0 \\ 0 & 0 & -1 \end{bmatrix} \end{matrix} \quad \begin{matrix} R_Y(\pi) \\ \begin{bmatrix} -1 & 0 & 0 \\ 0 & +1 & 0 \\ 0 & 0 & -1 \end{bmatrix} \end{matrix} \quad \begin{matrix} R_Z(\pi) \\ \begin{bmatrix} -1 & 0 & 0 \\ 0 & -1 & 0 \\ 0 & 0 & +1 \end{bmatrix} \end{matrix}.$$

The product of any two is the third. The square of each is the identity.

3.1. Invariant polynomials

Invariant polynomials are unchanged under the action of each of the operations of the symmetry group [1, 8]. Every function that is invariant under the group action can be expressed as a function of a small set of basic invariant polynomials. These basic invariant polynomials are the proper tool to use to construct relations between symmetric dynamical systems and their invariant image dynamical systems.

The four basic invariant polyonmials with $\mathbf{V}_4$ symmetry are

$$p_1 = X^2, \qquad p_2 = Y^2, \qquad p_3 = Z^2, \qquad p_4 = XYZ.$$

The quartic invariants are all products of quadratic invariants. The four basic invariant polynomials above are not independent, but obey one relation (syzygy) [1, 8]

$$(X^2)(Y^2)(Z^2) - (XYZ)^2 = p_1p_2p_3 - p_4^2 = 0.$$

The generating function for the number of invariants $N(d)$ of degree d is [1, 8]

$$\begin{aligned} f(x) &= \sum N(d)x^d \\ &= \frac{1}{4}\sum_{g_i} \frac{1}{\det[I_3 - x\mathbf{R}(g_i)]} = \frac{1+x^3}{(1-x^2)^3}. \end{aligned}$$

This shows that there are three independent quadratic terms (X^2, Y^2, Z^2), and that the cubic term obeys the syzygy $p_4^2 = p_1p_2p_3$ [8].

3.2. Invariant coordinates

It is useful to establish a $4 \to 1$ local diffeomorphism of $(X, Y, Z) \in \mathbb{R}^3(\boldsymbol{X})$ onto $(u_1, u_2, u_3) \in \mathbb{R}^3(\boldsymbol{u})$ using the following three linear combinations of the four basic quadratic and cubic invariant polynomials

$$\begin{aligned} u_1 &= \tfrac{1}{2}(X^2 - Y^2) \\ u_2 &= \tfrac{1}{2}(X^2 + Y^2 - 2Z^2) \\ u_3 &= XYZ. \end{aligned} \tag{2}$$

Every point in $\mathbb{R}^3(\boldsymbol{u})$ has four inverse images in $\mathbb{R}^3(\boldsymbol{X})$. They are obtained from

$$\begin{aligned} X &= \pm\sqrt{Z^2 + u_2 + u_1} \\ Y &= \pm\sqrt{Z^2 + u_2 - u_1}. \end{aligned} \tag{3}$$

The value of Z is determined from

$$u_3 = \sqrt{Z^2 + u_2 + u_1}\,\sqrt{Z^2 + u_2 - u_1}\,Z.$$

This equation has a unique solution, as can easily be seen. If $u_3 > 0$, the solution is in the positive octant $(X, Y, Z) = (+, +, +)$. If $u_3 < 0$, the solution is in the octant $(+, +, -)$. The unique solution with $u_1 > 0, u_2 > 0$ is mapped into the three additional inverse images by the three rotation operations

$$\begin{array}{cccccc} & & \mathbb{I} & R_X(\pi) & R_Y(\pi) & R_Z(\pi) \\ (+\,+\,+) & \to & (+\,+\,+) & (+\,-\,-) & (-\,+\,-) & (-\,-\,+) \\ (+\,+\,-) & \to & (+\,+\,-) & (+\,-\,+) & (-\,+\,+) & (-\,-\,-). \end{array}$$

The four inverse images in $\mathbb{R}^3(\boldsymbol{X})$ in the top line map to the upper half ($u_3 > 0$) of $\mathbb{R}^3(\boldsymbol{u})$. The bottom line maps to the lower half of this space.

3.3. The Jacobian

The relation between the equations of motion that are invariant under $\mathbf{V}_4$ and the image equations is given by a simple change of coordinate transformation. This transformation is effected by a Jacobian.

The Jacobian of the $4 \to 1$ local diffeomorphism of $\mathbb{R}^3(\boldsymbol{X})$ onto $\mathbb{R}^3(\boldsymbol{u})$ is

$$\frac{\partial \boldsymbol{u}}{\partial \boldsymbol{X}} = \begin{bmatrix} X & -Y & 0 \\ X & Y & -2Z \\ YZ & ZX & XY \end{bmatrix} \xrightarrow{\det} 2(X^2Y^2 + Y^2Z^2 + Z^2X^2).$$

The determinant vanishes when any two of the three quadratic invariants X^2, Y^2, Z^2 are zero. Specifically, the singular set of the determinant is

$$\begin{array}{ccccc} Y^2 + Z^2 = 0 & \cup & Z^2 + X^2 = 0 & \cup & X^2 + Y^2 = 0 \\ R_X(\pi) & & R_Y(\pi) & & R_Z(\pi). \end{array}$$

In short, it is the union of three rotation axes. The algebraic singularities reflect the geometric symmetry of the group.

3.4. Covering equations

The relation between the symmetric dynamical system $\dot{\mathbf{X}} = F(\mathbf{X})$ and the image dynamical system $\dot{\mathbf{u}} = f(\mathbf{u})$ is given by the chain rule:

$$\frac{\mathrm{d}\mathbf{u}}{\mathrm{d}t} = f(\mathbf{u}) = \frac{\partial \mathbf{u}}{\partial \mathbf{X}} \frac{\mathrm{d}\mathbf{X}}{\mathrm{d}t} = \frac{\partial \mathbf{u}}{\partial \mathbf{X}} F(\mathbf{X}).$$

In particular, the invariant functions $f(\mathbf{u})$ and equivariant functions $F(\mathbf{X})$ are related by

$$f(\mathbf{u}) \begin{bmatrix} X & -Y & 0 \\ X & Y & -2Z \\ YZ & ZX & XY \end{bmatrix} F(\mathbf{X}).$$

For $\mathbf{G} = \mathbf{V}_4$, the inverse of this relation gives

$$\begin{bmatrix} \dot{X} \\ \dot{Y} \\ \dot{Z} \end{bmatrix} = \frac{1}{\rho^2} \begin{bmatrix} X(Y^2 + 2Z^2) & XY^2 & YZ \\ -Y(X^2 + 2Z^2) & X^2Y & ZX \\ Z(X^2 - Y^2) & -Z(X^2 + Y^2) & XY \end{bmatrix} \begin{bmatrix} \dot{u}_1 \\ \dot{u}_2 \\ \dot{u}_3 \end{bmatrix},$$

where $\rho^2 = X^2Y^2 + Y^2Z^2 + Z^2X^2$.

A strange attractor in the image space can be lifted to a covering attractor in either of two ways. An initial condition in $\mathbb{R}^3(\mathbf{u})$ can be chosen and the image equations $\dot{\mathbf{u}} = f(\mathbf{u})$ can be integrated. The trajectory $\mathbf{u}(t)$ is then lifted into $\mathbb{R}^3(\mathbf{X})$ using equation (3). One trajectory in $\mathbb{R}^3(\mathbf{u})$ lifts to four not necessarily different trajectories in $\mathbb{R}^3(\mathbf{X})$. On the other hand, an initial condition in $\mathbb{R}^3(\mathbf{X})$ can be chosen and the symmetric equations $\dot{\mathbf{X}} = F(\mathbf{X})$ integrated directly.

3.5. Topological index

A symmetric dynamical system can be mapped to an image dynamical system, and the image is unique. This is not true in the reverse direction. An image dynamical system, and the strange attractor it creates, can be lifted to many different symmetric dynamical systems [1, 2]. The corresponding strange attractors can be topologically inequivalent, even though they all possess the same symmetry. The different lifts, and strange attractors, are distinguished by an index.

This index has three interpretations. At the topological level, the index is expressed in terms of the properties of an important subset of orbits in the image attractor. These are the period-1 orbits, one of which lies in each branch of the branched manifold that can be used to characterize the image strange attractor. The index is a set of integers. These describe how often each of the period-1 orbits circles around each of the rotation axes. For example, if a period-1 orbit in the image attractor is labelled 0 and it lifts to an orbit in the cover that encircles the X-axis once, then $n_{0X} = 1$. The index of a lift is the set of integers, for all period-1 orbits in the image, and all rotation axes of the symmetry group.

When the rotation axis or axes do not intersect the image, the lift is topologically unchanged under perturbations (structurally stable). When the axis or axes do intersect the image, the lifts are structurally unstable and undergo perestroikas. They are described below in section 3.8 and in [11].

The $\mathbf{V}_4$-symmetric covers of the Rössler image attractor are distinguished by the linking numbers of the period-1 orbits 0, 1 with the three rotation axes. The topological index in this

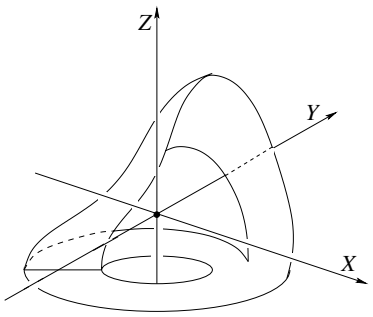

	X	Y	Z
0	0	0	1
1	0	1	1

Figure 1. Shown are a branched manifold for the Rössler attractor image and the X-, Y- and Z-rotation axes for the symmetry group $\mathbf{V}_4$. The period-1 orbit in the orientation preserving branch 0 links the three rotation axes with linking numbers $\mathbf{n}_0 = (0, 0, 1)$ and the period-1 orbit in the orientation reversing branch 1 links the three rotation axes with linking numbers $\mathbf{n}_1 = (0, 1, 1)$.

case is a six-component object:

$$\boldsymbol{n} = [n_x, n_y, n_z] = [(n_{0X}, n_{1X}), (n_{0Y}, n_{1Y}), (n_{0Z}, n_{1Z})].$$

	Axis		
Branch	X	Y	Z
0	n_{0X}	n_{0Y}	n_{0Z}
1	n_{1X}	n_{1Y}	n_{1Z}.

In figure 1, we show a Rössler-like image chaotic attractor and three rotation axes of a $\mathbf{V}_4$ symmetry group. Both the orientation preserving (0) and orientation reversing (1) branches encircle the Z-axis with a linking number 1 and the X-axis with a linking number 0. The orientation reversing branch does not circle the Y-axis, while the orientation reversing branch does. The topological index for this lift of the original Rössler-like image attractor is also shown in figure 1.

The image contains one branch line, so the cover contains four branch lines, each labelled by a group operation. In figure 2, we show how the branch lines in the cover are labelled. Branch line I is the branch line of the image Rössler branched manifold, as seen from above projected onto the X–Y plane. It lies below the plane in the third quadrant. The branch line labelled X is obtained by applying the group operation $R_Z(\pi)$ to the branch line I. It lies in the second quadrant above the X–Y plane. The other two branch lines are obtained similarly: Y in quadrant IV above the $Z = 0$ plane and Z in quadrant I below the $Z = 0$ plane. Each branch line in the cover has two parts: 0_γ, 1_γ, where $\gamma \in \mathbf{V}_4$. Initial conditions on the half-branch lines labelled 0 map onto the orientation preserving branch labelled 0 in the image under the $4 \to 1$ local diffeomorphism of equation (2); those labelled 1_γ map to orientation reversing branch 1 in the image.

We illustrate how the flow in the cover is determined by an example for the lift shown in figure 1. The period-1 orbit 0 in the image does not circle the X- or Y-axis, but does circle the Z-axis. It lifts to a segment of an orbit starting at half-branch 0_I and terminates on branch Z. As a result, the image of the half-branch line $0_{\mathbb{I}}$ under the flow is the branch line in $R_Z : 0_Z, 1_Z$. Similarly, the images of the other symbols 0_* under the flow are $R_Z 0_* = 0_{R_{Z^*}}, 1_{R_{Z^*}}$. Here $*$ is some group operation and the group product R_{Z^*} is well defined. The period-1 orbit 1 does not circle the X-axis but circles both the Y- and Z-axes. The image of the half-branch line $1_{\mathbb{I}}$ under the flow is $R_Y R_Z 1_{\mathbb{I}} = 0_{R_Y R_Z \mathbb{I}}, 1_{R_Y R_Z \mathbb{I}} = 0_X, 1_X$. In a similar way, the images of the

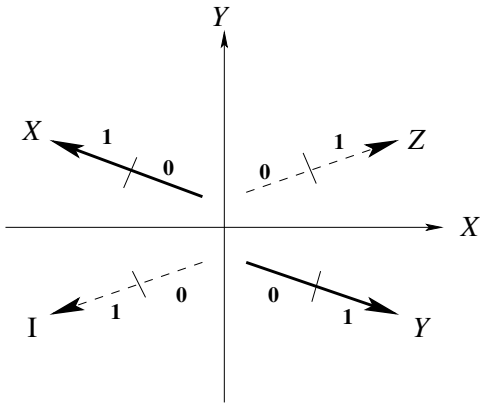

Figure 2. Labelling of the four different branch lines of the $\mathbf{V}_4$ cover of the Rössler system. Branch line I is the branch line of the image attractor. The other three are obtained by applying each of the three remaining group operations $R_X(\pi)$, $R_Y(\pi)$, $R_Z(\pi)$ to I.

other three symbols are $R_Y R_Z 1_X = (0, 1)_{\mathbb{I}}$, $R_Y R_Z 1_Y = (0, 1)_Z$, $R_Y R_Z 1_Z = (0, 1)_Y$. These results are summarized as follows:

$$\begin{aligned} &0_{\mathbb{I}} \to 0_Z, 1_Z \qquad && 1_{\mathbb{I}} \to 0_X, 1_X \\ &0_X \to 0_Y, 1_Y \qquad && 1_X \to 0_{\mathbb{I}}, 1_{\mathbb{I}} \\ &0_Y \to 0_X, 1_X \qquad && 1_Y \to 0_Z, 1_Z \\ &0_Z \to 0_{\mathbb{I}}, 1_{\mathbb{I}} \qquad && 1_Z \to 0_Y, 1_Y. \end{aligned} \tag{4}$$

3.6. Transition matrix

The index has an algebraic interpretation as well as a topological interpretation. The algebraic interpretation provides a description of how the flow is distributed among the branch lines. Specifically, each branch line can be divided into subsets (e.g., $\mathbb{I} \to (0, 1)_{\mathbb{I}}$), and each subset can be considered as a source of initial conditions that flow to another branch line. This geometric information can be encoded into a transition matrix. The transition matrix is the algebraic interpretation of the index.

The transition matrix for the $\mathbf{V}_4$-symmetric cover described in the previous subsection is

		$\mathbb{I}$		R_X		R_Y		R_Z	
		0	1	0	1	0	1	0	1
$\mathbb{I}$	0	0	0	0	0	0	0	1	1
	1	0	0	1	1	0	0	0	0
R_X	0	0	0	0	0	1	1	0	0
	1	1	1	0	0	0	0	0	0
R_Y	0	0	0	1	1	0	0	0	0
	1	0	0	0	0	0	0	1	1
R_Z	0	1	1	0	0	0	0	0	0
	1	0	0	0	0	1	1	0	0.

(5)

This transition matrix is simply a transcription of the information contained in equation (4).

For this topological index the cover is connected. This can be seen at two levels: every branch line is visited from an initial condition on any branch line, and the transition matrix

cannot be put in a block-diagonal form by a similarity transformation of the form $T' = PTP^{-1}$, where P is a permutation matrix.

The eigenvalues of this transition matrix are (2, 0, 0, 0, 0, 0, 0, −2). The topological entropy is log 2. More generally, the topological entropy of an image strange attractor is the same as the topological entropy of any of its **G**-symmetric covers, independent of the finite group **G** and the index chosen.

In a different case, we can choose topological index

	X	Y	Z
0	0	0	1
1	0	0	0.

(6)

For this index, the transition matrix is

		$\mathbb{I}$		R_X		R_Y		R_Z	
		0	1	0	1	0	1	0	1
$\mathbb{I}$	0	0	0	0	0	0	0	1	1
	1	1	1	0	0	0	0	0	0
R_X	0	0	0	0	0	1	1	0	0
	1	0	0	1	1	0	0	0	0
R_Y	0	0	0	1	1	0	0	0	0
	0	0	0	0	0	1	1	0	0
R_Z	0	1	1	0	0	0	0	0	0
	1	0	0	0	0	0	0	1	1.

(7)

This cover is disconnected. The branch lines $\mathbb{I}$, Z are connected by the transition matrix. They are mapped into each other by the subgroup (I, R_Z). The branch lines X and Y are also connected to each other under the flow, and mapped to each other under the same subgroup. The two pairs of branch lines $(\mathbb{I}, R_Z)$ and (R_X, R_Y) are disconnected from each other. Another way to see that the cover is disconnected is to observe that the transition matrix T is fully reducible into the direct sum of two irreducible transition matrices by a permutation group operation.

3.7. Group index

The index can also be expressed in the language of group theory. In order to provide all the connectivity information needed to describe the cover, it is sufficient to provide information about the image of the flow starting from the branch line $\mathbb{I}$. If the image branched manifold has two branches, this information is provided by two group operations. For the index whose topological representation is given in figure 1 and whose algebraic representation is given by the transition matrix in equation (5), the group index is $(g_1, g_2) = (R_Z, R_X)$ (cf also equation (4)). This is to be interpreted as follows: the half-branch line $\mathbb{I}_0$ flows to branch line $Z = R_Z\mathbb{I}$ and the half-branch line $\mathbb{I}_1$ flows to branch line $X = R_X\mathbb{I}$. For the index whose topological representation is given in equation (6) and whose algebraic representation is given by the transition matrix in equation (7), the group index is $(g_1, g_2) = (R_Z, \mathbb{I})$. In general, if the image branched manifold has b branches, there are $|\mathbf{G}|^b$ ways to choose the index.

The connectivity properties of a cover can be determined from the group representation of the index. The group operations, g_1 and g_2 above, generate a subgroup $\mathbf{H} \subset \mathbf{G}$. All branch lines that are mapped into each other under this subgroup **H** are connected under the flow, and disconnected from other subsets. The disconnected subsets are identified by the coset

representatives $\mathbf{G}/\mathbf{H}$. The $|\mathbf{G}|/|\mathbf{H}|$ subsets can be identified by certain group elements in $\mathbf{G}$ that are not in $\mathbf{H}$. These are called coset representatives [2].

As a result, the connectivity of each component is labelled by a set of group operations that generate a subgroup, and the set of different disconnected components is also labelled by a set of group operations that identify a coset.

3.8. Spectrum of $\mathbf{V}_4$*-symmetric covers*

The Smale horseshoe branched manifold (cf figure 1 and [1, 2, 5, 6]) can be lifted to many different $\mathbf{V}_4$ symmetric covers: $|\mathbf{G}|^2 = 4^2 = 16$ indices are possible. For several choices of indices the following results occur:

Index (g_1, g_2)	Subgroup $\mathbf{H}$	$\mathbf{G}/\mathbf{H}$ Coset Representatives	# Com− ponents
(I, I)	I	$\{I, R_x, R_Y, R_Z\}$	4
(I, R_X)	$\{I, R_X\}$	$\{I, R_Y\}$	2
(R_Y, R_Y)	$\{I, R_Y\}$	$\{I, R_X\}$	2
(R_X, R_Y)	$\{I, R_X, R_Y, R_Z\}$	I	1

(8)

The 16 four-fold covers of the Smale horseshoe branched manifold with $\mathbf{V}_4$ symmetry are partitioned as follows:

	Symbol	Index								
$\mathbf{V}_4$	0	$\mathbb{I}$	$\mathbb{I}$	$\mathbb{I}$	$\mathbb{I}$	R_X	R_Y	R_Z	R_X	R_Y	R_Z
	1	$\mathbb{I}$	R_X	R_Y	R_Z	$\mathbb{I}$	$\mathbb{I}$	$\mathbb{I}$	R_X	R_Y	R_Z
		4-components	2-components								

	Symbol	Index					
$\mathbf{V}_4$	0	R_X	R_Y	R_Z	R_X	R_Z	R_Y
	1	R_Y	R_Z	R_X	R_Z	R_Y	R_X
		Connected covers					

(9)

The cover $(0, 1) \to (\mathbb{I}, \mathbb{I})$ consists of four disconnected components. The next nine, $(0, 1) \to (\mathbb{I}, R_X)$ through (R_Z, R_Z), consist of two disconnected components. There are three dual pairs: $(\mathbb{I}, R_X) \leftrightarrow (R_X, \mathbb{I})$, etc and three self-dual covers: (R_X, R_X), etc. For example, the cover with index $(0, 1) \to (\mathbb{I}, R_Z)$ has one component containing branch lines $\mathbb{I}$ and R_Z, while the symmetry-related component (under either R_X or R_Y) contains branch lines R_X and R_Y. Similarly for the self-dual cover $(0, 1) \to (R_Z, R_Z)$. The three covers with indices $(\mathbb{I}, R_X)$, $(\mathbb{I}, R_Y)$, $(\mathbb{I}, R_Z)$ are related to each other by rotations about the $(1, 1, 1)$ axis by $2\pi/3$ radians, i.e., by the group $\mathbf{C}_3$.

The remaining six covers consist of a single connected component. There is a path in each of these branched manifolds from any branch line to any other branch line. There are three dual pairs, such as $(R_X, R_Y) \leftrightarrow (R_Y, R_X)$. In addition, the first three (R_X, R_Y), (R_Y, R_Z), (R_Z, R_X) are mapped into each other under $\mathbf{C}_3$, as are the last three in this list. If we regard the symmetry-related attractors (under $\mathbf{C}_3$) as essentially equivalent, the

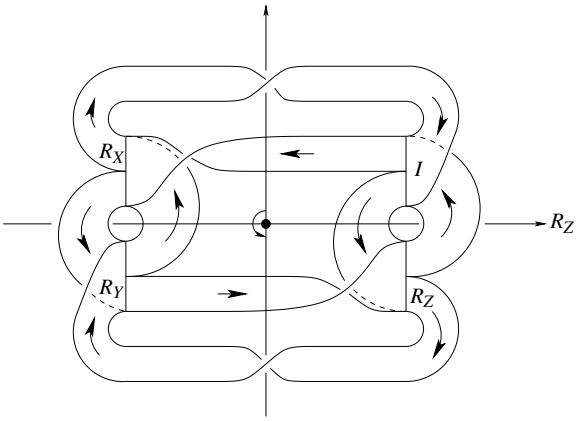

Figure 3. Branched manifold of the $\mathbf{V}_4$ cover of the Rössler system with an index shown in figure 1. This branched manifold is a planar projection of a $\mathbf{V}_4$-symmetric branched manfiold.

breakdown of distinct $\mathbf{V}_4$-invariant covers of Smale horseshoe dynamics is

♯ Components	♯ Dual pairs	♯ Self-dual pairs
4	0	$1(\mathbb{I}, \mathbb{I})$
2	$1(\mathbb{I}, R_X)$	$1(R_X, R_X)$
1	$1(R_X, R_Y)$	0.

In summary, there are six $(= 2 \times (0 + 1 + 1) + 1 \times (1 + 1 + 0))$ topologically distinct types of covers of the basic Smale horseshoe branched manifold with $\mathbf{V}_4$ symmetry.

4. Systems with $\mathbf{V}_4$ symmetry

In this section, we describe how to create $\mathbf{V}_4$-symmetric lifts of the Rössler equations with a previously specified index. We describe how periodic orbits in the Rössler attractor lift to periodic orbits in the symmetric covers. Finally, we review two dynamical systems that have $\mathbf{V}_4$-equivariant forcing terms.

4.1. V_4 cover of the Rössler system

The Rössler attractor can be lifted to a cover with $\mathbf{V}_4$ symmetry and index given in figure 1. The cover branched manifold has $\mathbf{V}_4$ symmetry. It is difficult to represent this branched manifold in planar projection. For this reason, a topologically accurate distortion is presented in figure 3.

We start from the modified Rössler system

$$\begin{aligned} \dot{x} &= -z - y - \mu_z - \mu_y \\ \dot{y} &= x + a(y + \mu_y) + \mu_x \\ \dot{z} &= b(x + \mu_x) + (z + \mu_z)(x - c + \mu_x), \end{aligned} \tag{10}$$

where (a, b, c) are the usual parameter values and (μ_x, μ_y, μ_z) are used to located the rotation axes properly.

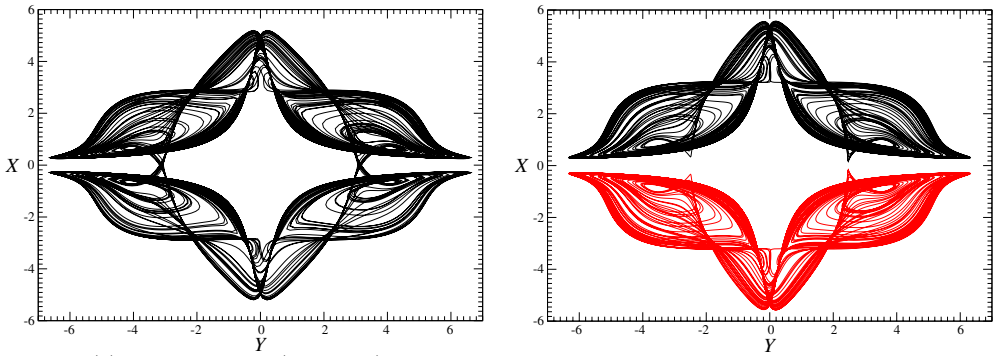

(*a*) One component ($\mu_x = 1.80$)

(*b*) Two components ($\mu_x = -0.84$)

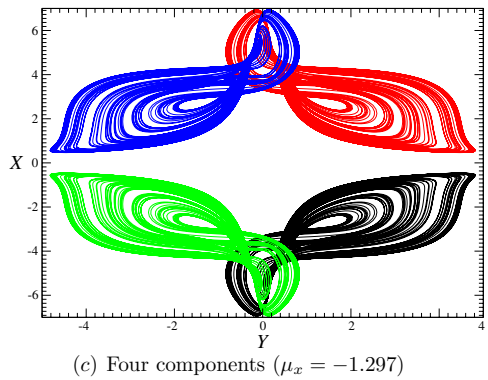

(*c*) Four components ($\mu_x = -1.297$)

Figure 4. $\mathbf{V}_4$-symmetric covers of the Rössler attractor. The topology (connectedness) of the cover changes with the index, which changes as the control parameter μ_x is varied. Parameter values: $(a, b, c) = (0.420, 2.0, 4.0)$.

The $\mathbf{V}_4$ cover is built using the dynamical equation

$$\begin{aligned}
\dot{X} &= \frac{X(Y^2 + 2Z^2)\dot{x} + XY^2\dot{y} + 2YZ\dot{z}}{2\rho^2} \\
\dot{Y} &= \frac{-Y(X^2 + 2Z^2)\dot{x} + X^2Y\dot{y} + 2XZ\dot{z}}{2\rho^2} \\
\dot{Z} &= \frac{Z(X^2 - Y^2)\dot{x} - Z(X^2 + Y^2)\dot{y} + 2XY\dot{z}}{2\rho^2},
\end{aligned} \tag{11}$$

where $\rho^2 = X^2Y^2 + X^2Z^2 + Y^2Z^2$.

We vary μ_x and use $(\mu_y, \mu_z) = (-1.0, 1.0)$. Covering attractors with three different topological indices are shown in three different projections in figure 4. The attractor shown in figure 4(*a*) is connected. It has only one component. This component is invariant under the entire group $\mathbf{V}_4$. The attractor in figure 4(*b*) consists of two connected components. Each is invariant under the subgroup $\{\mathbb{I}, R_Y(\pi)\}$ and each is mapped into its symmetric partner by the two group operations $\{R_X, R_Z\}$. The two components are labelled by the coset representatives $\mathbb{I}$ and R_X (or R_Z). The attractor shown in figure 4(*c*) consists of four disconnected components, each invariant under the subgroup $\mathbb{I}$. They are mapped into each

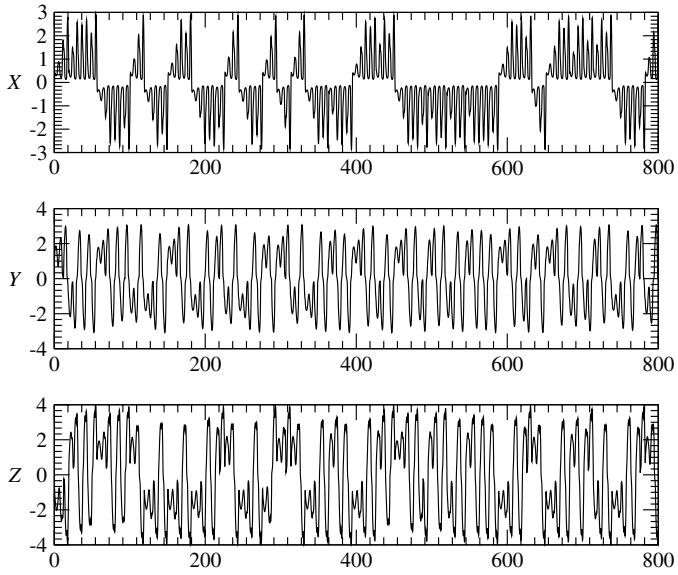

Figure 5. The time series for the connected $\mathbf{V}_4$-symmetric cover of the Rössler attractor shown in figure 4(*b*).

other by the full group $\mathbf{G}/\mathbf{H} = \mathbf{V}_4/\mathbb{I}$. The coset representatives that identify each of the four disconnected components are the group operations $\mathbb{I}$, R_X, R_Y, R_Z.

The time series for the three coordinates $X(t)$, $Y(t)$, $Z(t)$ are shown in figure 5 for the connected attractor shown in figure 4(*a*). The connectivity of the attractor can be inferred from the time series, assuming the time series of the image Rössler attractor is known. For the image attractor, the $u_1(t)$ and $u_2(t)$ time series oscillate about a single fixed point. For the time series shown in figure 5, the time series $Y(t)$ oscillate about two symmetrically placed values of Y_0. The time series $Z(t)$ also oscillates about two values of Z_0. Further, these oscillations are incoherent, so that the Y–Z coordinates of the fixed points are $(\pm Y_0, \pm Z_0)$. As a result, the phase-space trajectory visits four unstable foci, so the attractor must consist of a single connected component.

4.2. Periodic orbits

Periodic orbits in the image can be lifted to the cover following the prescription provided in figure 1 [2]. The two period-3 orbits 100 and 101 in the Rössler attractor are shown in figure 6. This figure also shows the location of the $u_3 = Z$ rotation axis that is used to lift the image to the cover with topological index given in figure 1. The lifts of these two period-3 orbits into the covering attractor with this topological index are shown in figure 7. In each case, the period-3 orbits lift to a pair of symmetry-related period-6 orbits. The two lifts of 100 are invariant under $\{\mathbb{I}, R_Y\}$, while the two lifts of 101 are invariant under a different symmetry subgroup, $\{\mathbb{I}, R_Z\}$.

The symbolic name of the lifts can be determined systematically [2]. We do this for the lift of 100. We first write out the three-symbol sequence 100 several times: 100 100 100 .... Then we initiate a flow from branch line $\mathbb{I}$. This is done by assigning the subscript $\mathbb{I}$ to the symbol 1: $1_{(\mathbb{I},*)}$. The flow from this part of the branch line $\mathbb{I}$ then goes to the branch line

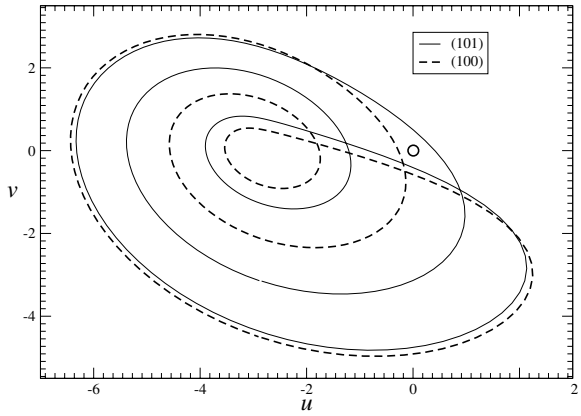

Figure 6. Period-3 orbits embedded within the Rössler attractor. The rotation axis (○) is located between them. Thus the lifts of the orbits are organized in a different way in the cover space $\mathbb{R}^3(X, Y, Z)$.

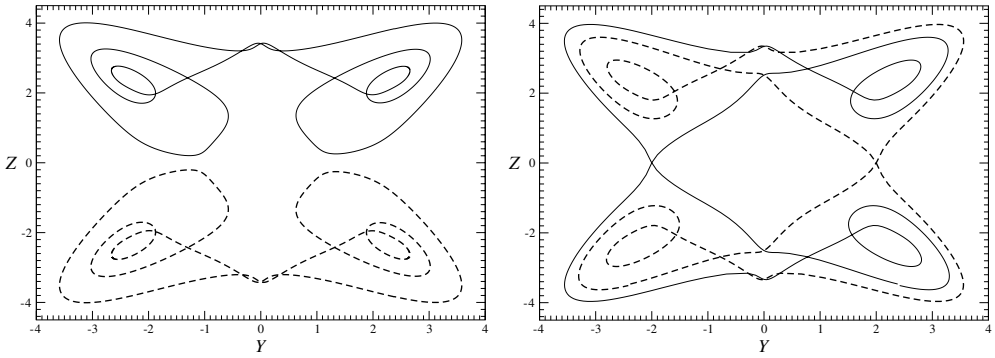

(*a*) (100) (*b*) (101)

Figure 7. Covers of the period-3 orbits extracted from the Rössler system for $a = 0.432$. Pairs of periodic orbits are shown in the Y–Z plane projection. The cover is shown in figure 4(*a*). Although the covering attractor is connected, the lift of each period-3 orbit consists of a symmetry-related pair of period-6 orbits.

R_X, as seen from the transition matrix in equation (5). This provides us with the information $1_{(\mathbb{I},R_X)}0_{(R_X,*)}$. The transition matrix shows that 0_{R_X} flows to R_Y, so that the symbol sequence is now $1_{(\mathbb{I},R_X)}0_{(R_X,R_Y)}0_{(R_Y,*)}$. From the transition matrix, the symbol $*$ is R_X. This does not bring us back to the starting branch line $\mathbb{I}$, so this iterative process continues for three more symbols (at least). The algorithm ends when the second group label for the $3n$th symbol is the same as the first group label for the first symbol (starting point). For the orbit 100 and the index chosen, this occurs at the 6th symbol, so one lift of 100 is an orbit of period 6. There is a second lift of 100 that is obtained from the first by a group operation ($\gamma = R_Y$). The symbol names of the lifts of the period-3 pair 100, 101 in the image attractor are

$$100 \rightarrow \begin{array}{l} 1_{(\mathbb{I},R_X)}0_{(R_X,R_Y)}0_{(R_Y,R_X)}1_{(R_X,\mathbb{I})}0_{(\mathbb{I},R_Z)}0_{(R_Z,\mathbb{I})} \\ 1_{(R_Y,R_Z)}0_{(R_Z,\mathbb{I})}0_{(\mathbb{I},R_Z)}1_{(R_Z,R_Y)}0_{(R_Y,R_X)}0_{(R_X,R_Y)} \end{array}$$

$$101 \to \begin{array}{l} 1_{(\mathbb{I},R_X)}0_{(R_X,R_Y)}1_{(R_Y,R_Z)}1_{(R_Z,R_y)}0_{(R_Y,R_X)}1_{(R_X,\mathbb{I})} \\ 1_{(R_X,R_Y)}0_{(R_Y,R_X)}1_{(R_X,R_Y)}1_{(R_Y,R_Z)}0_{(R_Z,\mathbb{I})}1_{(\mathbb{I},R_X)}. \end{array}$$

Each period-3 orbit in the image lifts to a pair of period-6 symmetry-related orbits in the cover. The two pairs of lifts have different symmetry groups. The symmetry group of an orbit in the cover can be determined simply and algorithmically.

4.3. Normal form equations for $\mathbf{V}_4$*-equivariant systems*

Dynamical systems invariant under $\mathbf{V}_4$ can be constructed systematically from the ring of covariant polynomials. Every polynomial in X, Y, Z can be expressed in terms of invariant functions (functions of the basic invariant polynomials X^2, Y^2, Z^2, XYZ), the invariant 1, and the covariant polynomials X, Y, Z and XY, YZ, ZX [8]. The pair (X, YZ) of covariant polynomials transform identically under all group actions. The same is true for (Y, ZX) and (Z, XY). Therefore, a $\mathbf{V}_4$ invariant dynamical system can always be written in terms of $\mathbf{V}_4$-equivariant functions as

$$\begin{aligned} \dot{X} &= F_{11}X + F_{12}YZ \\ \dot{Y} &= F_{21}Y + F_{22}ZX \\ \dot{Z} &= F_{31}Z + F_{32}XY. \end{aligned} \tag{12}$$

The $F_{i\alpha}$ are functions of the four basic invariant polynomials.

Two $\mathbf{V}_4$-equivariant systems have previously been proposed. Both have this form, with all functions $F_{i\alpha}$ constant. These are treated now.

4.4. Liu and Chen system

Liu and Chen proposed a system with $\mathbf{V}_4$ symmetry [12]:

$$\begin{aligned} \dot{X} &= aX + YZ \\ \dot{Y} &= -bY - ZX \\ \dot{Z} &= -cZ - XY. \end{aligned} \tag{13}$$

We hold $a = 0.5$ and $b = 12.0$ fixed and treat c as a bifurcation parameter. It has one degenerate fixed point located at the origin of the phase space. Its eigenvalues are $\lambda_1 = a$, $\lambda_2 = -b$ and $\lambda_3 = -c$. It is a saddle. There are four other fixed points located at

$$\begin{aligned} X_\pm &= \pm\sqrt{bc} \\ Y_\pm &= \pm\sqrt{ac} \\ Z_\pm &= \pm\sqrt{ab}, \end{aligned} \tag{14}$$

where the product of these three coordinates is negative. If a, b or c is negative, the fixed points are imaginary. If a, b and c are positive, they are saddle foci with one negative real eigenvalue. With $c = 4$, two attractors co-exist in the phase space (figure 8(*a*)). Their image is shown in figure 8(*b*).

4.5. Lü, Chen and Cheng system

Lü, Chen and Cheng have proposed a similar system with $\mathbf{V}_4$ symmetry [13]:

$$\begin{aligned} \dot{X} &= -\frac{ab}{a+b}X - YZ \\ \dot{Y} &= aY + XY + v \\ \dot{Z} &= bZ + XY. \end{aligned} \tag{15}$$

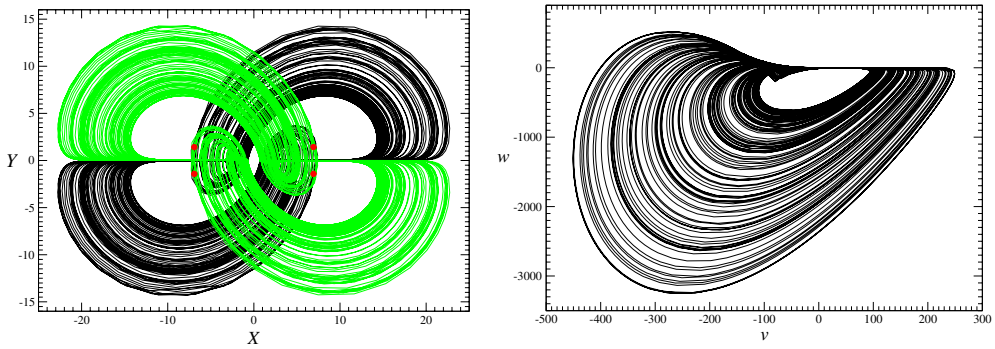

(*a*) Phase portrait of the symmetric attractor (*b*) Image attractor

Figure 8. (*a*) Chaotic attractor for the Liu–Chen system has $\mathbf{V}_4$ symmetry and two disconnected components. (*b*) Both have the same image. Parameter values: $(a, b, c) = (0.5, 12.0, 4.0)$.

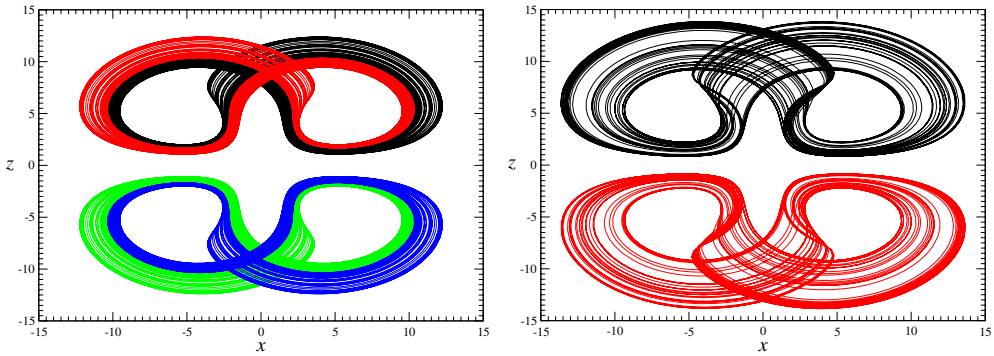

(*a*) Four components ($b = -2.4170$) (*b*) Two components ($b = -2.5305$)

Figure 9. (*a*) Chaotic attractors for the Lü–Chen–Cheng system with (*a*) 4- and (*b*) 2-components. Parameter values: $(a, v) = (-10, 0)$.

This system has $\mathbf{V}_4$ symmetry when $v = 0$. In this case, the system has five fixed points. One is located at the origin of the phase space $\mathbb{R}^3(X, Y, Z)$. The four other fixed points are symmetry related and are

$$F_{1,\pm}\mathbf{X} = \begin{vmatrix} X = \pm\sqrt{ab} \\ Y = \pm|b|\sqrt{\frac{a}{a+b}} \\ Z = \pm a\sqrt{\frac{b}{a+b}} \end{vmatrix} \tag{16}$$

subject to the condition that the product of the three coordinates is $XYZ = -a^2b|b|/(a+b)$. One parameter a is fixed at $a = -10$ and b is varied over the interval $[-2.34, -5.604]$. When $b = -2.4170$, four components are observed (figure 9(*a*)). Each of the four components of the chaotic attractor is topologically equivalent to a Burke and Shaw attractor with two branches before the attractor-merging crisis [3]. When b is decreased, an attractor-merging crisis occurs and symmetry-related pair of attractors remains in the phase space when $b = -2.5305$ (figure 9(*b*)). Each is topologically equivalent to the Burke and Shaw attractor characterized by a four-branch return map.

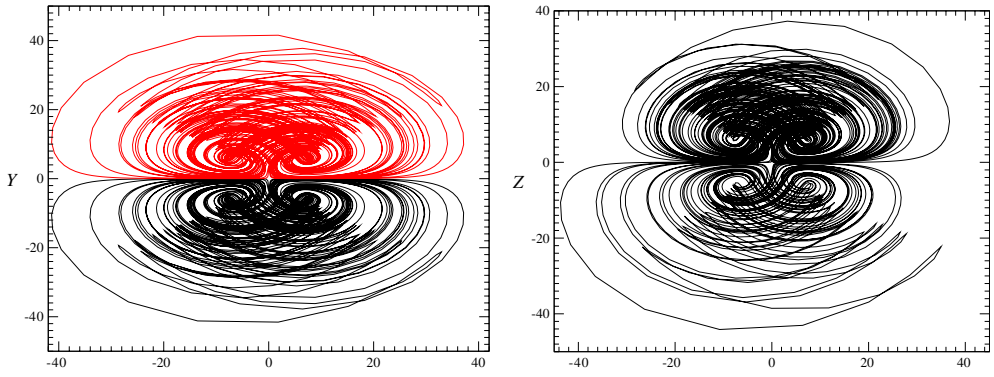

(*a*) Two components ($\nu = 0.0$) (*b*) One component ($\nu = 1.0$)

Figure 10. (*a*) Chaotic attractor with $\mathbf{V}_4$ symmetry for the Lü–Chen–Cheng system has two components and (*b*) one component when the symmetry is broken ($\nu \neq 0$). Parameter values: $(a, b) = (-10, -4.417)$.

When parameter b is further decreased, the attractor continues to grow, as observed for the Burke and Shaw system. Note that the trajectory never crosses the plane defined by $Z = 0$ (figure 10(*a*)). This is only permitted when a perturbation is added. For instance, when $\nu = 1.0$, the trajectory crosses the plane $Z = 0$ and a one-component attractor is observed (figure 10(*b*)).

5. $\mathbf{S}_4$ symmetry

At the abstract level, there are two groups of order 4. One has a single generator A that satisfies the single relation: $A^4 = I$. The four group operations are $\{I, A, A^2, A^3\}$. The other group (four-group, or viergruppe) has two generators A and B that satisfy three relations: $A^2 = I, B^2 = I$ and $AB = BA$. The four group operations are $\{I, A, B, AB\}$. We have discussed one representation of the four group in $\mathbb{R}^3$ extensively in the previous two sections.

The cyclic group has two different representations in $\mathbb{R}^3$. The matrix representatives of the generator A in these two representations are

$$\begin{array}{cc} C_4 & S_4 = \sigma_Z C_4 \\ \begin{bmatrix} 0 & 1 & 0 \\ -1 & 0 & 0 \\ 0 & 0 & 1 \end{bmatrix} & \begin{bmatrix} 0 & 1 & 0 \\ -1 & 0 & 0 \\ 0 & 0 & -1 \end{bmatrix}. \end{array} \tag{17}$$

The group $\mathbf{C}_4$ with the generator C_4 consists of rotations about the Z-axis through multiples of $\pi/2$ radians. The generator S_4 describes a rotation about the Z-axis through $\pi/2$ radians followed by a reflection in the $Z = 0$ plane. The groups with generator C_4 and S_4 are called $\mathbf{C}_4$ and $\mathbf{S}_4$, respectively.

5.1. Leipnik and Newton system

Leipnik and Newton proposed a system with three quadratic interactions arising from Euler's rigid body equations modified by the addition of linear feedback [14]. The equations are

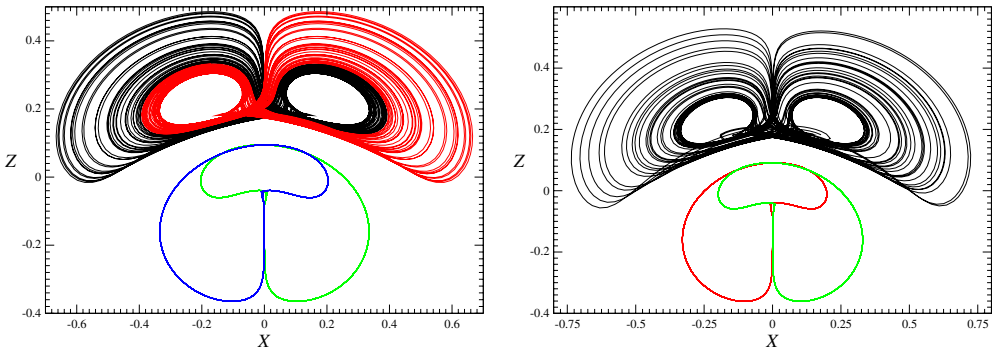

(*a*) Four disconnected attractors ($c = 0.15134$) (*b*) Three disconnected attractors ($c = 0.152$)

Figure 11. The Leipnik and Newton system has attractors with (*a*) four and (*b*) three disconnected components and $R_Z(\pi)$ symmetry. Some components are chaotic, others are stable limit cycles. Parameter values: $(a, b) = (0.73, 5)$.

$$\begin{aligned} \dot{X} &= -aX + Y + 2bYZ \\ \dot{Y} &= -X - aY + bZX \\ \dot{Z} &= -bXY + cZ. \end{aligned} \tag{18}$$

This system has a $R_Z(\pi)$ rotation symmetry. There are five fixed points. One is located at the origin of the phase space and the four others are

$$F_{\pm\pm} = \begin{vmatrix} X_\pm = \pm\dfrac{\sqrt{2ac\,(A \pm B)}}{b\,(\pm 3 + B)} \\ Y_\pm = \pm\dfrac{\sqrt{2ac\,(A \pm B)}}{4ab} \\ Z_\pm = \pm\dfrac{\sqrt{2ac\,(A \pm B)}}{bc\,(\pm 3 + B)}, \end{vmatrix} \tag{19}$$

where $A = 3 + 4a^2$ and $B = \sqrt{9 + 8a^2}$. For certain parameter values, four attractors co-exist in the phase space as shown in figure 11(*a*). The two disconnected attractors observed mainly with positive Z values are topologically equivalent to the Burke and Shaw strange attractor observed before the first attractor-merging crisis. When the initial conditions are changed, two limit cycles also co-exist in the phase space for mostly negative Z values. These two cycles remain roughly unchanged when the c parameter is increased to 0.152. During this process, the two disconnected attractors with mostly positive Z values merge into a single strange attractor (figure 11(*b*)). The total attractor has three disconnected components.

The two attractors with negative Z values are different from the two attractors with positive Z values, because a higher ($\mathbf{S}_4$) symmetry is broken by the factor 2 in the term $2bYZ$ in the first equation of system (18). The $\mathbf{S}_4$ symmetry can be imposed by replacing the coefficient 2 in the first part of equations (13) by 1. Thus, for $(a, b, c) = (0.60, 5, 0.1428)$, four disconnected symmetry-related attractors are obtained. Their projections on the X–Z and X–Y planes are shown in figure 12. For values of c greater than 0.1428, the attractors merge and two disconnected attractors remain in the phase space. Both are symmetry related.

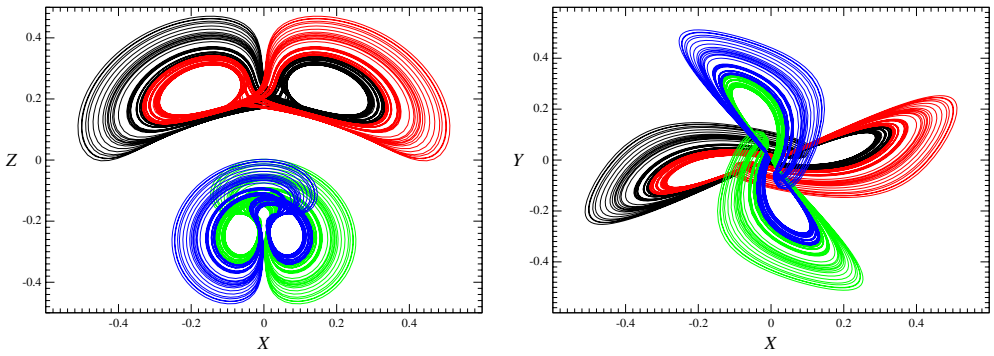

(*a*) X-Z plane projection (*b*) X-Y plane projection

Figure 12. The modified ($2 \to 1$) Leipnik and Newton system exhibits four disconnected chaotic attractors for parameter values $(a, b, c) = (0.60, 5, 0.1428)$.

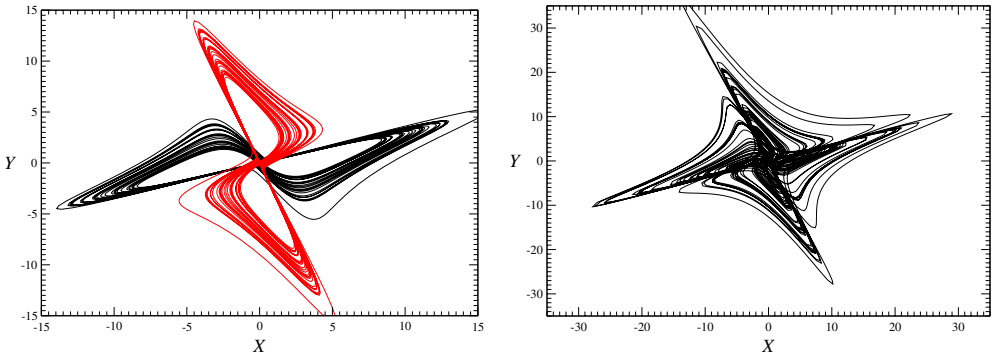

(*a*) Two disconnected components ($a = -2.0$) (*b*) A single component ($a = -2.45$)

Figure 13. The Chechin and Ryabov equations exhibit $\mathbf{S}_4$ invariant strange attractors with (*a*) two disconnected components and (*b*) a single component. Parameter value: $b = 1$.

5.2. Chechin and Ryabov system

In investigating discrete symmetries, Chechin and Ryabov [15] introduced a new system with a $\mathbf{S}_4$ symmetry. The equations are

$$\begin{aligned} \dot{X} &= aX + bY - XZ - YZ \\ \dot{Y} &= -bX + aY - XZ + YZ \\ \dot{Z} &= Z + XY. \end{aligned} \tag{20}$$

This system has five fixed points. One is located at the origin of the phase space and the four others are symmetry related. When $a = -2.0$ and $b = 1$, there are two disconnected components (figure 13(*a*)) which are topologically equivalent to the Lorenz attractor (a cusp return map can be easily obtained). When the a parameter is slightly decreased, an attractor-merging crisis occurs and a single attractor remains in the phase space (figure 13(*b*)).

In their investigation, Chechin and Ryabov proposed another set of equations with a $\mathbf{S}_4$ symmetry. They are

$$\begin{aligned}\dot{X} &= aX + Y - XZ \\ \dot{Y} &= -X - aY + YZ \\ \dot{Z} &= Z + (X^2 - Y^2) + XY.\end{aligned} \tag{21}$$

These equations behave similarly to system (20).

6. $\mathbf{S}_6$ symmetry

The group $\mathbf{S}_6$ consists of rotations by $2\pi/6$ radians about a symmetry axis, followed by reflection in a plane perpendicular to that axis. In $\mathbb{R}^3$, this can be implemented in a very symmetric way by choosing the axis in the (1, 1, 1) direction. The group generator γ has the simple form $(x, y, z) \to (-y, -z, -x)$, with $\gamma^3 = -\mathbb{I}$ and $\gamma^6 = \mathbb{I}$.

6.1. Covering equations

Equations that are equivariant under this group have the form

$$\dot{x}_i = c_{ij}x_j + c_{ijk}x_jx_k + c_{ijkl}x_jx_kx_l + \cdots, \tag{22}$$

where $1 \leqslant i, j, \ldots \leqslant 3$. Invariance of the equations requires $c_{i+1,j+1} = +c_{i,j}$, $c_{i+1,j+1,k+1} = -c_{i,j,k}$, $c_{i+1,j+1,k+1,l+1} = +c_{i,j,k,l}$, etc. In short, coefficients of the linear and cubic (and odd) terms are constrained, and those of the quadratic and quartic (and even) terms are zero.

6.2. Thomas system

A system with an $\mathbf{S}_6$ symmetry has been proposed by Thomas [16]

$$\begin{aligned}\dot{x} &= -bx + ay - y^3 \\ \dot{y} &= -by + az - z^3 \\ \dot{z} &= -bz + ax - x^3.\end{aligned} \tag{23}$$

For this system, $c_{11} = c_{22} = c_{33} = -b, c_{12} = a, c_{12^3} = -1$ and the remaining nonzero coefficients are obtained by cyclic permutation of the indices.

6.3. Fixed points

For all values of (a, b), the origin $(x, y, z) = (0, 0, 0)$ is a fixed point. It is six-fold degenerate. The Jacobian is the cyclic matrix

$$\mathbf{J} = \begin{bmatrix} -b & a & 0 \\ 0 & -b & a \\ a & 0 & -b \end{bmatrix}. \tag{24}$$

with eigenvalues $-b + a\epsilon^j$, where $\epsilon = \mathrm{e}^{2\pi \mathrm{i}/3}$ and $j = 0, 1, 2$. There are two fixed points along the (1, 1, 1) rotation axis at $x = y = z = \pm\sqrt{a - b}$. The eigenvalues at these fixed points are $-b + (3b - 2a)\epsilon^j$.

In general, this system has 36 fixed points, counting degeneracy. For $b = 0.3$ and $a = 1.1$, they are all real and tabulated below. The fixed point F_0 at the origin is six-fold degenerate.

The two fixed points F_I on the axis (1, 1, 1) are each three-fold degenerate. The sets F_{II}–F_V each consist of six symmetry-related points.

	x	y	z
F_0	0.0000	0.0000	0.0000
F_I	$\pm$0.8944	$\pm$0.8944	$\pm$0.8944
	$\pm$1.0370	$\pm$0.3098	$\pm$0.0850
F_{II}	$\pm$0.0850	$\pm$1.0370	$\pm$0.3098
	$\pm$0.3098	$\pm$0.0850	$\pm$1.0370
	$\pm$1.0128	$\pm$0.8653	$\pm$0.2502
F_{III}	$\pm$0.2502	$\pm$1.0128	$\pm$0.8653
	$\pm$0.8653	$\pm$0.2502	$\pm$1.0128
	$\pm$1.0953	$\mp$1.1746	$\mp$0.3643
F_{IV}	$\mp$0.3643	$\pm$1.0953	$\mp$1.1746
	$\mp$1.1746	$\mp$0.3643	$\pm$1.0953
	$\pm$1.1796	$\pm$0.8164	$\mp$1.1461
F_V	$\mp$1.1461	$\pm$1.1796	$\pm$0.8164
	$\pm$0.8164	$\mp$1.1461	$\pm$1.1796.

The eigenvalues for these fixed points are

F_I	$\lambda_{1,2} = +0.35 \pm 1.1258I$
	$\lambda_3 = -1.6$
F_{II}	$\lambda_{1,2} = +0.31506 \pm 1.0653I$
	$\lambda_3 = -1.5301$
F_{III}	$\lambda_{1,2} = -.93704 \pm 1.1034I$
	$\lambda_3 = +0.97409$
F_{IV}	$\lambda_{1,2} = -1.1734 \pm 1.5128I$
	$\lambda_3 = +1.4469$
F_V	$\lambda_{1,2} = +0.69404 \pm 1.7217I$
	$\lambda_3 = -2.2880.$

All of these fixed points are either stable foci with an unstable perpendicular direction or unstable foci with a stable perpendicular direction.

6.4. A projection with high symmetry

In order to have a better representation of the symmetry properties, we use the coordinate transformation

$$\begin{aligned} X &= \frac{\sqrt{3}}{2}(y - x) \\ Y &= z - \frac{x + y}{2} \\ Z &= x + y + z. \end{aligned} \tag{25}$$

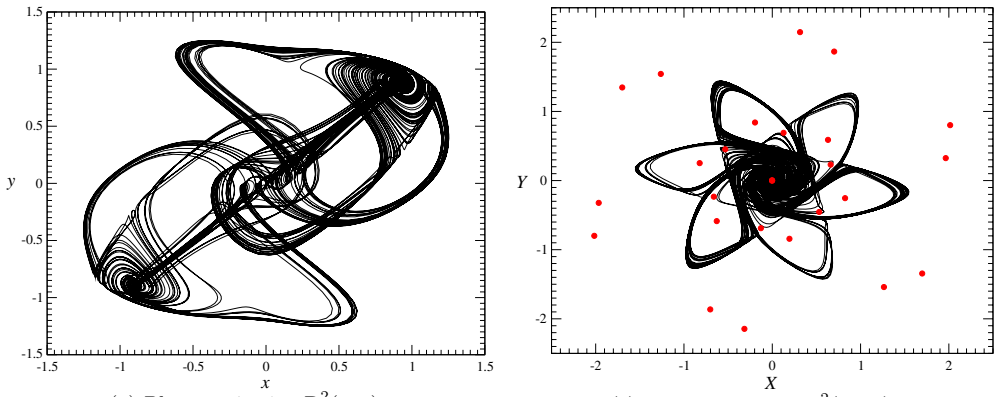

(*a*) Plane projection $\mathbb{R}^2(x, y)$ (*b*) Plane projection $\mathbb{R}^2(X, Y)$

Figure 14. A single attractor generated by the Thomas system for $a = 1.1$. The 27 fixed points are shown in the plane projection $\mathbb{R}^2(X, Y)$. Note that points F_I cannot be distinguished from the point located at the origin of the projection $\mathbb{R}^2(X, Y)$.

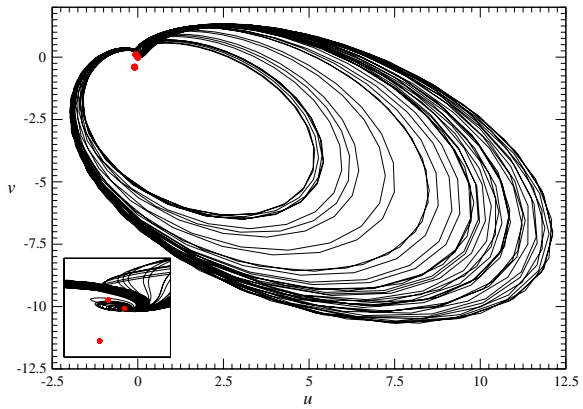

Figure 15. Image of the single attractor generated by the Thomas system for $a = 1.1$.

The Z-axis is the (1, 1, 1) rotation axis while the (X, Y) coordinates parametrize the plane through the origin perpendicular to the rotation axis. Projection of the attractor onto the X–Y plane clearly shows the six-fold symmetry of the dynamical system. For example, a single connected attractor for $(a, b) = (1.1, 0.3)$ is shown in the x–y projection in figure 14(a) and X–Y plane in figure 14(b). The locations of all the fixed points are shown in the latter projection where their symmetry is apparent.

A projection of the $6 \mapsto 1$ image (figure 15) is obtained using the coordinate transformation

$$\begin{aligned} u &= \Re(X + \mathrm{i}Y)^6 \\ &= X^6 - 15X^4Y^2 + 15X^2Y^4 - Y^6 \\ v &= \Im(X + \mathrm{i}Y)^6 \\ &= 6X^5Y - 20X^3Y^3 + 6XY^5. \end{aligned} \tag{26}$$

This projection is shown in figure 15.

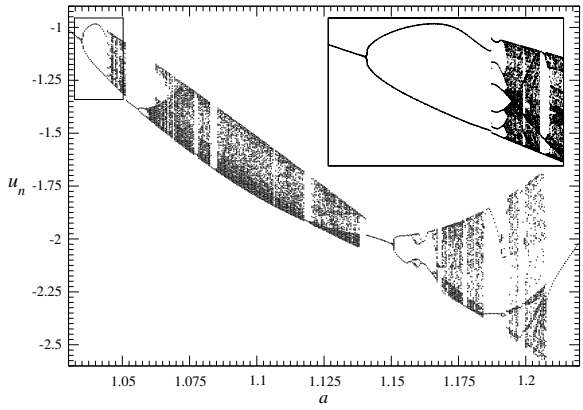

Figure 16. Bifurcation diagram for the Thomas system versus a for $b = 0.3$. The diagram is actually constructed for the image attractor.

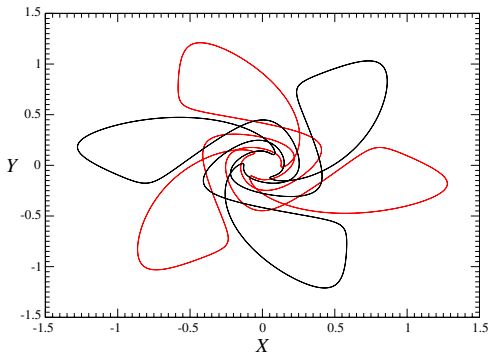

(a) 2 period-1 limit cycles for $a = 1.030000$

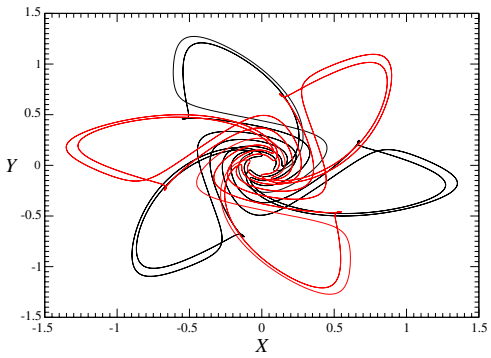

(b) 2 period-2 limit cycles for $a = 1.044193$

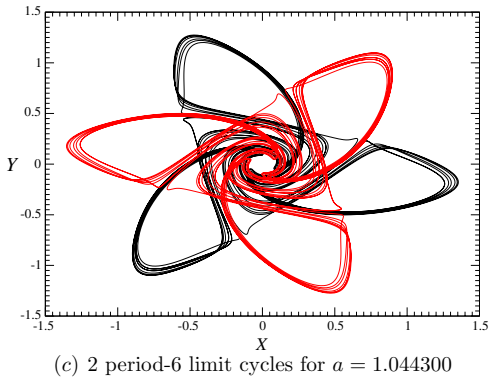

(c) 2 period-6 limit cycles for $a = 1.044300$

Figure 17. Thomas dynamical system. Different pairs of limit cycles co-exist in the phase space.

6.5. Bifurcation studies

We study the bifurcations of the dynamical system along the line $b = 0.3$, $1.01 \leqslant a \leqslant 1.22$ in the control parameter plane. The bifurcation diagram for the equivariant system (23) is

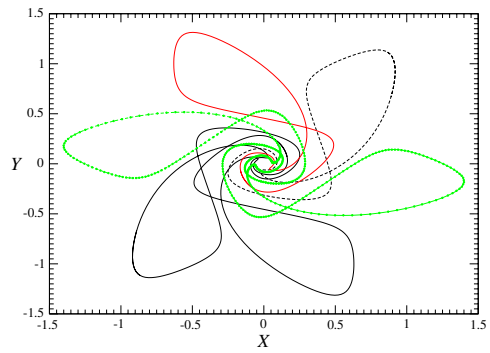

(*a*) 6 period-1 limit cycles for $a = 1.0550$

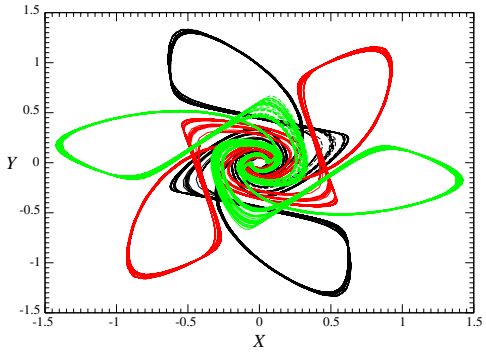

(*b*) 6 coexisting chaotic attractors for $a = 1.0623$

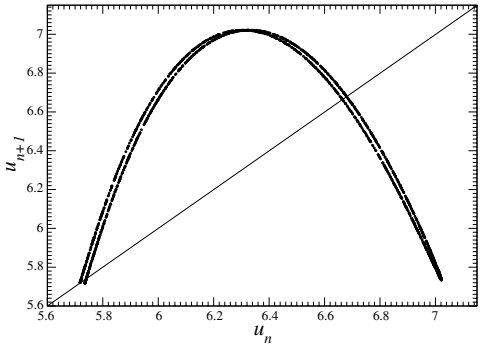

(*c*) First-return map of an attractor for $a = 1.0623$

Figure 18. Thomas dynamical system. (*a*) Six period-1 limit cycles produce six simultaneous period-doubling cascades leading to (*b*) six co-existing attractors. (*c*) First return map for the image dynamical system shows a complete symbolic dynamics on two symbols.

complicated and difficult to understand. The bifurcation properties of the $6 \mapsto 1$ image are *much* simpler to visualize and interpret. The two systems are locally diffeomorphic; therefore, very little information is lost in studying the simpler bifurcation diagram. The bifurcation diagram for the image system is given in figure 16.

This bifurcation diagram shows that the image attractor has a period-1 orbit at $a = 1.03$, a period-2 orbit at $a = 1.044\,193$, a period-6 orbit at $a = 1.044\,300$ (see inset in figure 16). Another period-1 orbit at $a = 1.0550$, and a chaotic attractor at $a = 1.0623$. These are covered by two or six attractors in the $\mathbf{S}_6$-equivariant system. The first three limit cycles are shown in figures 17(*a*)–(*c*). The six period-1 limit cycles at $a = 1.0550$ and the six disconnected strange attractors they create through a period-doubling cascade are shown in figures 18(*a*) and (*b*). The first return map on the image coordinate u is shown in figure 18(*c*). This unimodal map shows that the image attractor exhibits a complete symbolic dynamics on two symbols, that is, it is a horseshoe.

7. Conclusion

We have presented a systematic way to construct dynamical systems with a particular symmetry group. This procedure involves construction of polynomials invariant under the action of the group, and functions of these invariant polynomials. The complementary polynomials, called

covariant polynomials, are used to construct the equivariant functions in the invariant equations of motion. Invariant coordinates are introduced. These are linear combinations of the invariant polynomials. The invariant dynamical system is obtained from the equivariant system by this simple change of coordinates. The Jacobian of this transformation (chain rule) has singularities that reflect the singularities (the rotation axes) of the symmetry group.

Mapping an equivariant dynamical system to its image is straightforward. The image is unique. An image can be lifted to a symmetric cover. The lift is not unique, but identified by an index. This index has three related interpretations: topological, algebraic and group theoretical. Each interpretation provides different information about the cover, its properties, and the properties of the lifts of periodic orbits from the image dynamical system. An algorithm has been described and used to construct the symbolic name of the lifts into any cover (with any symmetry group) of periodic orbits in the image. This has been done explicitly for lifts of the two period-3 orbits 100 and 101 of the Rössler system into a covering system with the symmetry group $\mathbf{V}_4$ with a specified index.

These procedures have been used to describe the properties of equivariant dynamical systems with symmetry groups $\mathbf{V}_4$, $\mathbf{S}_4$ and $\mathbf{S}_6$. These include the structure of the equivariant functions for the symmetric equations and their image equations. We show that bifurcation diagrams for image dynamical systems are much simpler to construct than for their symmetric covers.

Acknowledgments

RG is supported in part by NSF grant PHY 9987468. A part of this work was done during a stay by CL at Drexel University and another part during a stay by RG at the Université de Rouen, CORIA.

References

[1] Letellier C and Gilmore R 2001 *Phys. Rev.* E **63** 16206
[2] Gilmore R and Letellier C 2003 *Phys. Rev.* E **67** 036205
[3] Letellier C, Dutertre P, Reizner J and Gouesbet G 1996 *J. Phys. A: Math. Gen.* **29** 5359
[4] Miranda R and Stone E 1993 *Phys. Lett.* A **178** 105
[5] Gilmore R and Lefranc M 2002 *The Topology of Chaos* (New York: Wiley)
[6] Gilmore R 1998 *Rev. Mod. Phys.* **70** 1455
[7] Tsankov T and Gilmore R 2003 *Phys. Rev. Lett.* **91** 134104
[8] Cox D, Little J and O'Shea D 1996 *Ideals, Varieties and Algorithms: An Introduction to Computational Algebraic Geometry and Commutative Algebra* (Berlin: Springer)
[9] Rössler E 1976 *Phys. Lett.* A **57** 397
[10] Abraham R and Marsden J E 1978 *Foundations of Mechanics* 2nd edn (New York: Benjamin)
[11] Letellier C, Tsankov T, Byrne G and Gilmore R 2005 *Phys. Rev.* E **72** 026212
[12] Liu W and Chen G 2003 *Int. J. Bifurcation Chaos* **13** 261
[13] Lü J, Chen G and Cheng D 2004 *Int. J. Bifuraction Chaos* **14** 1507
[14] Leipnik R and Newton T 1981 *Phys. Lett.* A **86** 63
[15] Chechin G and Ryabov D 2004 *Phys. Rev.* E **69** 036202
[16] Thomas R 1999 *Int. J. Bifuraction Chaos* **9** 1889